Hindawi
International Journal of Optics
Volume 2022, Article ID 5830310, 8 pages
https://doi.org/10.1155/2022/5830310

Research Article

Design and Numerical Analysis of a Single-Polarization Filter Based on PCF with Plasmonic Layers of Gold and Indium Tin Oxide

Isaac Owusu Mensah,[1,2] **Emmanuel Kofi Akowuah**,[1] **Iddrisu Danlard**,[1] **and Alexander Kwasi Amoah**[1]

[1]*Departmentof Computer Engineering, Kwame Nkrumah University of Science and Technology, Kumasi, Ghana*
[2]*Department of Communication Engineering, Carinthia University of Applied Science, Klagenfurt, Austria*

Correspondence should be addressed to Isaac Owusu Mensah; isaac.owusumensah@edu.fh-kaernten.ac.at

Received 22 October 2021; Revised 16 February 2022; Accepted 23 March 2022; Published 7 April 2022

Academic Editor: haochong huang

This paper presents a single-polarization filter based on PCF with plasmonic layers of gold and indium tin oxide (ITO). The plasmonic materials are metallic gold and ITO coated on the inner walls of two extra-large vertically arranged air holes. The resonance effect is triggered by guided modes propagating through the silica core and coupling to the coating areas. The finite element method is used to analyze the properties of the filter for the two fundamental orthogonal polarizations. A filtering effect is achieved in the communication window by optimizing the structural factors as well as gold film and ITO deposition thicknesses. When the filter is 1 mm long, the obtained filtering effect is 1319.689 dB/cm for the y-polarization and 31.881 dB/cm for the x-polarization, thus efficiently attenuating the y-component at a communication window of 1.15 μm. With a filtering bandwidth of 602 nm, the proposed filter shows superior characteristics compared with previously reported results. Applications of the proposed plasmonic PCF-based filter can be found in polarization-maintaining and polarization-suppressing systems for optical sensing and broadband transmission.

1. Introduction

Photonic crystal fibers (PCFs) have gained extensive attention in a variety of sectors in recent decades. PCFs are new forms of optical fibers in which arbitrary air hole shapes such as longitudinal [1], spiral [2], and elliptical [3] exist throughout the fiber. Several functional devices based on PCFs have been developed, including sensors [4], rotators [5], lasers [1], amplifiers [6], and polarization filters [7]. Polarization filters, in particular, are essential components in high-speed optoelectronic and communication infrastructure. These polarization filters are optical devices that discriminate by suppressing incident light based on polarization features and are commonly used to provide effective polarization state management [1, 2]. Efficient polarization filters are easily achieved on PCF platforms due to the tunability of their structural parameters, in addition to their small and compact size, as well as their insusceptibility to electromagnetic influence [8].

Due to their high sensitivity [9], partially or fully metalized PCFs have advanced rapidly in recent decades [10]. These can be made by infiltrating metal wires into the PCF air holes or by covering all or some selected inner walls of the air holes with single or multiple metal coatings [11]. With this arrangement, surface plasmon polaritons (SPPs) can occur on the metalized surfaces when light waves encroach the boundaries between the metalized sections and their dielectric surroundings. When the propagation constant of a particular SPP order and a core-guided wave become equal, the energy of the core-guided mode is transported to the

SPP, establishing the surface plasmon resonance (SPR) condition. In this case, there are noticeable peaks in the output loss spectrum.

Furthermore, due to the tunability of the structural parameters of PCFs, it is possible to obtain a tunable cross talk ratio and a broad wavelength working range. Chen et al. developed a polarization filter based on liquid crystal penetrated PCFs with a gold wire. At 1550 nm, the mode loss was 446 dB/cm for the y-polarization and 0.8 dB/cm for the x-polarization [12]. Zhao et al. designed a type of gold-coated PCF filter. At 1550 nm, the loss in the y-polarization was 906.9 dB/cm, which was much larger than the x-polarization of [13]. A polarization filter based on high-birefringence PCF with gold nanowires was constructed and numerically investigated by Du et al. In the communication windows of 1310 and 1550 nm, the observed losses were about 40 and 60 dB/cm [14]. Fan et al. used SPR effects to investigate the behavior of a D-shaped PCF-based polarization filter. The mode losses at 1310 and 1550 nm were 244.9 and 292.8 dB/cm, respectively [7]. Li et al. reported a single-polarization PCF-based narrow-width filter with mode losses of 330.75 and 242.89 dB/cm at 1310 nm and 1550 nm, respectively [15]. Yang et al. suggested a tunable polarization filter with polarization mode losses of 305.1 and 53.1 dB/cm based on a silver sheet filled with liquid. At 1.55 and 1.31 m, the other losses were 2.4 and 0.8 dB/cm, respectively. Very recently, Chang et al. introduced a high-birefringence gold-coated PCF polarization filter. There were six elliptical air holes and the cladding consisted of a solid core bounded by a three-layer regular hexagon cluster of circular air holes. Notably, the confinement loss of the y-polarized mode reached 442 dB/cm in the 1550 nm communication band, whereas the loss of the x-polarized mode was only 0.0316 dB/cm (Table 1).

Based on the preceding, it is clear that device performance enhancements such as competitive mode loss levels, crosstalk benchmarks, and filtering bandwidth are necessary. A single-polarization PCF filter is proposed and numerically evaluated in this paper. Within the walls of two extra-large, vertically arranged air holes of a PCF, dual layers of metallic gold and indium tin oxide (ITO) are deposited. The finite element method (FEM) is used to evaluate the filtering capabilities of the PCF filter. To achieve an optimal filtering performance, the influence of model parameters, GOLD, and ITO coating thickness are thoroughly investigated. The crosstalk performance and filtering bandwidth of the filter are also investigated.

2. Structural Design and Fundamental Theories

The sectional view of the PCF filter is presented in Figure 1(a). A three-dimensional view and the finite element mesh of the proposed filter are also shown in Figures 1(b) and 1(c), respectively. The structure of the filter consists of fractal layers of air holes organized into self-repeating patterns in vertical and horizontal transitions, respectively. The lattice pitch is designated as Λ and initially set at 1.60 μm. The diameters of the extra-large vertically disposed air holes are represented by d_1 with an initial value of 1.8 μm. Other air holes, including the elliptical ones, denoted as d_2, d_3, d_4, and d_5, d_x, and d_y are initially set to 0.6 μm, 1.6 μm, 1.0 μm, 0.5 μm, 0.3 μm, and 0.6 μm, respectively.

The proposed structure is inherently birefringent due to the different air hole sizes surrounding the core area. The placement of the two extra-large horizontal air holes makes the coating process of ITO and gold films on the inner walls more convenient. The ITO layers are represented by blue rings, while the gold layers are represented by yellow rings with thicknesses denoted by t_{ITO} and t_{GOLD}, respectively. Initially, $t_{ITO} = 10$ nm and $t_{GOLD} = 30$ nm.

The proposed can be actualized using current fabrication technologies such as stacking [23], extrusion [24], sol-gel casting [24], and drilling [25]. Small interhole distances can be maintained using high-precision ultrasonic drilling technology [25]. The preform can be drawn into fibers at the drawing tower [7]. The air hole sizes are controlled by manipulating the drawing speed and temperature [15]. Lastly, the plasmonic layers can be coated on the inner walls of the air holes by chemical vapor deposition [10] or sputtering technique [26].

The finite element method (FEM) in COMSOL® Multiphysics was used to investigate the performance characteristics of the proposed filter. A perfectly matched layer (PML) [27] was applied to demarcate the computational area and to prevent back reflections of scattered waves. The working wavelength range in this investigation is 1.0 μm–1.6 μm. The computational area was meshed into 10,770 elements. The mesh quality statistics include 33096 domain elements, 127 vertex elements, 2761 edge elements, and a minimum element quality of 0.3952. The refractive index of air was set at $n_{air} = 1$. The host material is silica, and its dispersion relation follows the Sellmeier equation as follows [28]:

$$n^2(\lambda) = 1 + \frac{0.6962\lambda^2}{\lambda^2 - 0.0047} + \frac{0.4079\lambda^2}{\lambda^2 - 0.0135} + \frac{0.8975\lambda^2}{\lambda^2 - 97.934}, \quad (1)$$

where n and λ are the refractive index of silica and the wavelength of light, respectively. The material dispersion of gold was calculated by the Drude–Lorentz model [29].

$$\varepsilon_m = \varepsilon_\infty - \frac{\omega_D^2}{\omega(\omega + j\gamma_D)} - \frac{\varepsilon \times \Omega_L^2}{\left(\omega^2 - \Omega_L^2\right) - j\omega\Gamma_L}, \quad (2)$$

where ε_∞ is the permittivity at infinite frequency, ε is a weighting factor, ω is the angular frequency of the interacting light, ω_D and γ_D are the plasma frequency and damping frequency, respectively, and Ω_L and Γ_L are the frequency and the spectral width of the Lorentz oscillator, respectively. Here, $\varepsilon_\infty = 5.9673$ is the permittivity the high frequency, $\Delta\varepsilon = 1.09$, $\omega_D/2\pi = 2113.6$ THZ, and $\gamma D/2\pi = 15.92$ THZ. Ω_L and Γ_L are the frequency and the spectral width of the Lorentz oscillator, respectively, $\Omega_L/2\pi = 650.07$ THZ, and $\Gamma_L/2\pi = 104.86$ THZ.

The permittivity of ITO was computed as follows [30]:

$$\varepsilon_m(\lambda) = \varepsilon_\infty - \frac{\lambda^2\lambda_c}{\lambda_p^2(\lambda_c + i\lambda)}, \quad (3)$$

Table 1: Comparisons of polarization filter performance.

PCF characteristics and reference	Communication window and loss	CT and filtering bandwidth	Fiber length
Asymmetric filter based on infiltrated PCF with gold coating [16]	1310 nm and 434 dB/cm	353.74 dB and 120 nm (about)	$L = 1$ mm
PCF-based filter with symmetrical gold-coated holes [17]	1550 nm and 431.267 dB/cm	180 dB (about) and 190 nm	$L = 0.5$ mm
High-birefringence PCF filter with gold wires [18]	1310 nm and 40 dB/cm 1550 nm and 60 dB/cm	N/A	N/A
PCF-based splitter with dual plasmonic inner air holes [10]	1310 nm and 102.6 dB/cm 1550 nm and 245.0 dB/cm	95 dB (about) and 40 nm 200 dB (about) and 100 nm	$L = 1$ mm
Symmetry-structured PCF polarization filter [19]	1310 nm and 231.6 dB/cm 1550 nm and 237.9 dB/cm,	240 dB and 60 nm 197 dB and 70 nm	$L = 1$ mm
D-shaped PCF polarization filter [20]	1310 nm and 244.9 dB/cm 1550 nm and 292.8 dB/cm	208.4 dB and 88 nm 249.5 dB and 150 nm	$L = 1$ mm
Single-polarization PCF filter with narrow bandwidth [21]	1310 nm and 330.75 dB/cm 1550 nm and 242.89 dB/cm	285.642 dB and 70 nm 202.92 dB and 235 nm	$L = 1$ mm
PCF-based filter with gold film on the inner wall of two ultralarge holes [22]	1550 nm and 569.682 dB/cm 1310 nm and 588.900 dB/cm 1550 nm and 971.330 dB/cm	494.673 dB and 700 nm 511.491 dB and 270 nm 843.622 dB and 630 nm	$L = 1$ mm
Single polarization filter based on PCF with plasmonic layers of gold and indium tin Oxide (our work)	1150 nm and 1319.6890 dB	72.05 dB and 602 nm	$L = 1$ mm

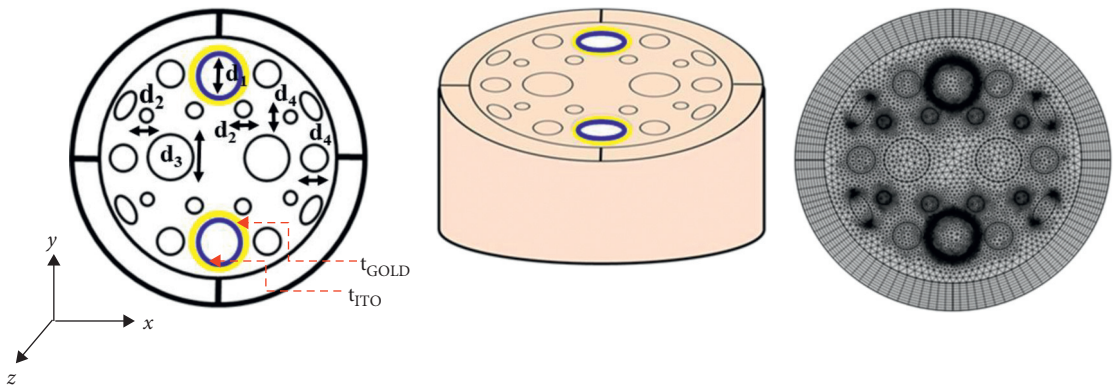

(a) (b) (c)

Figure 1: (a) A sectional view of the plasmonic PCF filter. (b) A three-dimensional representation. (c) The finite element mesh of the proposed filter.

where ε_∞ is the intraband dielectric constant for the infinite value of frequency, $\lambda_c = 11.21076 \times 10^6 = m$ is the collision wavelength for ITO, and $\lambda_c = 5.6497 \times 10^7\ m$ is the plasma wavelength for ITO. The mode confinement loss is a key benchmark for characterizing modal characteristics of filters. It can be expressed as follows [31, 32]:

$$\alpha_{\text{loss}}\left(\lambda, n_{eff}\right) = 8.686 \times \frac{2\pi}{\lambda} \text{Im}\left(n_{eff}\right) \times 10^4 \,(\text{dB/cm}), \quad (4)$$

where $\alpha_{\text{loss}}(\lambda, n_{eff})$ stands for confinement loss, λ specifies the operating wavelength, and $\text{Im}(n_{eff})$ represents the imaginary part of the complex refractive index of a guided mode. In the event of the phase of a core mode and that of an SPP mode matching, the core mode is usually strongly coupled to the SPP mode along the coated surface at a specific wavelength. Under this condition, the SPR effect is established. At the resonance wavelength, the mode confinement loss is the highest due energy transfer to the SPP modes. The structural parameters as well as the thicknesses of the gold and ITO films influence the resonance wavelength and loss.

3. Analysis of Numerical Results and Discussion

In Figure 2, the mode loss of the x- and y-polarizations as well as the dispersion relations between the y-polarization and the SPP modes is shown for $d_1 = 1.8\,\mu$m, $d_2 = 0.6\,\mu$m, $d_3 = 1.6\,\mu$m, $d_4 = 1.0\,\mu$m, $\Lambda = 1.6\,\mu$m, $t_{\text{ITO}} = 15$ nm, and $t_{\text{GOLD}} = 30$ nm. The confinement loss of the x- and y-

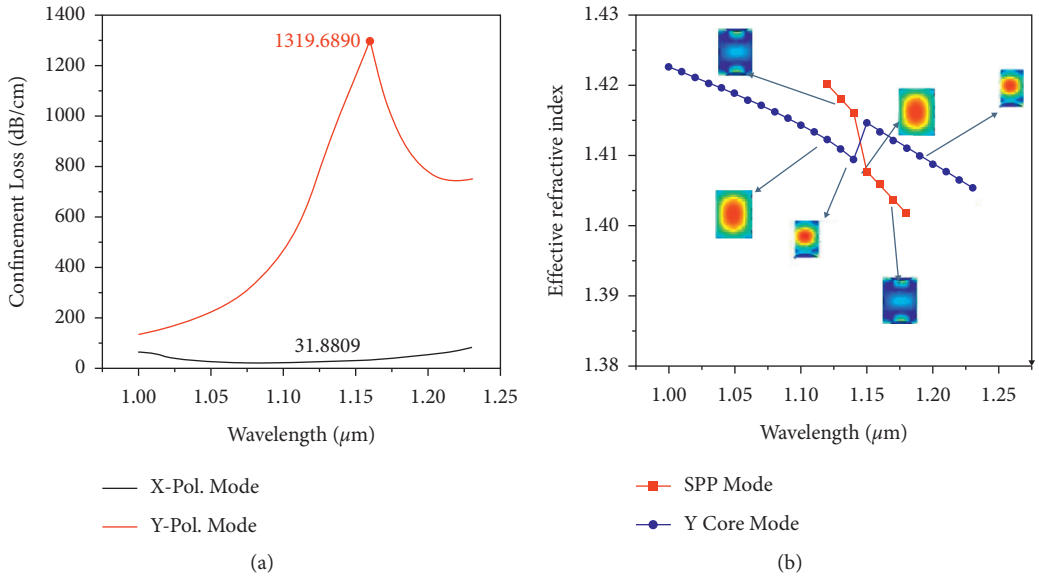

Figure 2: Dispersion relations of the y-polarized core modes and SPP modes.

polarized core modes is shown in Figure 2, with blue and red curves representing the loss spectrum of the x- and y-polarized core modes, respectively. The objective is to make the loss of desired polarized mode lower while increasing the loss of the undesired polarized mode.

At the resonance wavelength of 1.15 μm, the confinement losses of the x- and y-polarizations are 31.83 and 1319.689 dB/cm, respectively. In effective polarization filtering, the mode loss of the wanted mode should be much smaller when compared with that of the unwanted polarized mode. The y-polarization loss is only examined because the x-polarization loss is negligible in comparison to that of the y-polarization mode. Consequently, the dispersion relations of the y-polarized and SPP modes are depicted in Figure 2(b) (blue and red solid lines are the real part of the effective refractive indices of the y-polarized core mode and that of the SPP mode, respectively). Due to the SPR effect, the effective refractive index of the y-polarized core mode mutates and intersects with that of the SPP mode at the resonance wavelength of 1.15 μm. It can be observed that the core mode for the y-polarization diminishes first before strengthening in the wavelength range of 1.10–1.20 μm. The energy of the y-polarized core mode is at its lowest at 1.15 μm. Because the energy of the y-polarized state was evacuated to the SPP mode, the SPP mode is modified leading to plasmonic resonance at 1.15 μm. All other y-polarization states are coupled to the SPP modes in the same way.

3.1. Impact of Different Diameters on the Filtering Performance. Based on the cladding microstructure of the filter, the effective area of the core is controlled by the air hole sizes in the first ring. Consequently, the effects of d_2 and d_3 on the filtering characteristics are investigated to optimize the filtering performance. Figure 3(a) shows the loss spectra for different values of d_2 when $d_3 = 1.60\,\mu$m, $t_{ITO} = 15$ nm, and $t_{gold} = 30$ nm. When d_2 is varied from 0.4 μm to 0.8 μm, it is seen that as the loss peaks undergoes blueshift. Points of maximum loss are distinct for d_2 value of 0.4 μm, 0.5 μm, 0.6 μm, 0.7 μm, and 0.8 μm. At lower values of d_2, the losses do not vary considerably because smaller air hole sizes have insignificant influence on the effective refractive index of the silica background. The phase-matching (resonant) points appear at wavelengths of 1.17 μm, 1.16 μm, 1.16 μm, 1.13 μm, and 1.11 μm. Figure 3(b) illustrates variations of effective mode indices with varying d_2 when $d_3 = 1.60\,\mu$m, $t_{ITO} = 15$ nm, and $t_{GOLD} = 30$ nm. The intersection of the effective mode indices of each core-guided mode and its associated SPP mode is blue shifting with decreasing d_2.

Here, the resonances are redshifting and occur at 1.11 μm, 1.12 μm, 1.15 μm, 1.18 μm, and 1.24 μm, respectively, with corresponding losses of 1306.622, 1362.054, 1319.214, 1233.735, and 993.499 dB/cm. It is clear from Figure 4(a) that larger mode losses correspond to higher values of d_3 and vice versa. This is because as d_3 becomes large, the effective core area reduces, leading to decrease in the effective mode index of the core mode. Also, when d_3 increases, the effective refractive index of silica decreases significantly due to broadening of air hole inclusions. When compared with d_2, d_3 has a substantial influence on the loss profiles and resonant peaks shifts. In Figure 4(b), the effective mode indices for various values of d_3 are presented when $d_1 = 1.8\,\mu$m, $t_{ITO} = 15$ nm, and $t_{GOLD} = 30$ nm. The effective mode index of each guided mode traverses its associated SPP modes, causing the intersection to blueshift as d_3 decreases.

3.2. Impact of Various t_{GOLD} on the Filter's Response. The plasmonic layer thickness is an important factor in the polarization filter's performance. The impact of gold film thicknesses, t_{GOLD}, is investigated herein. The loss spectrum for the filter is shown in Figure 5 with various t_{GOLD} values in

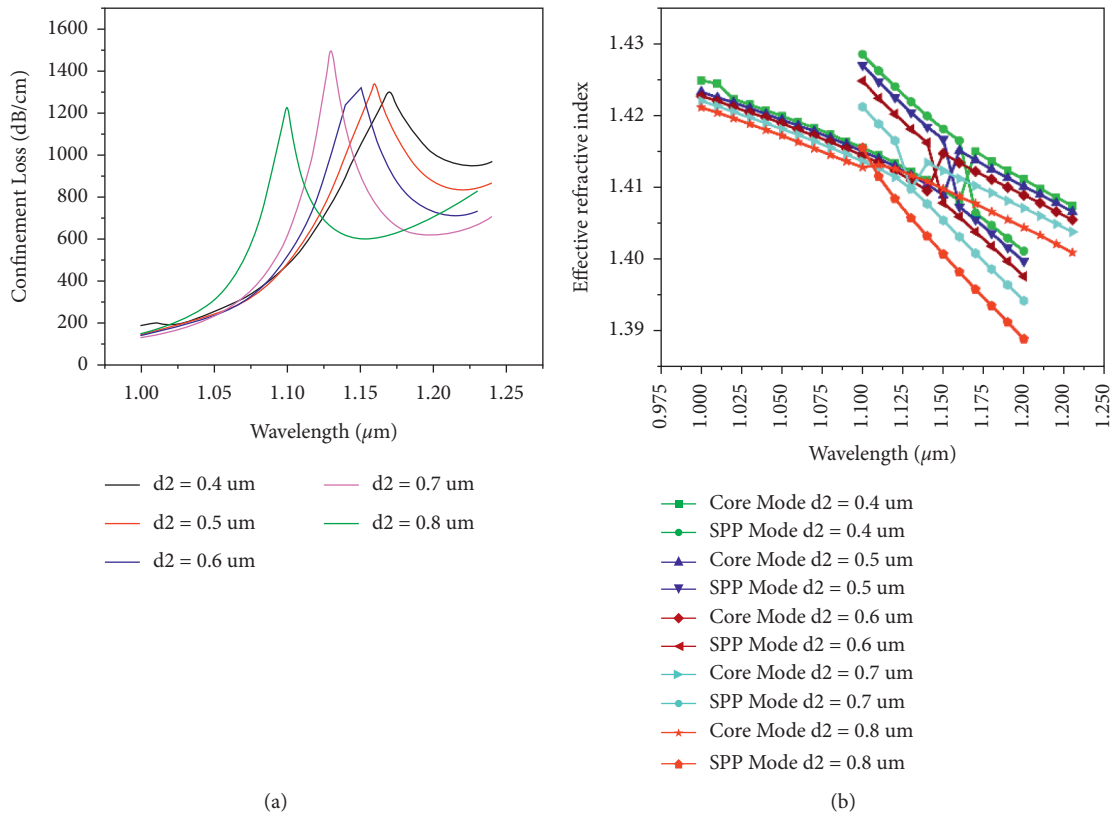

FIGURE 3: (a) The loss spectra and (b) the effective mode index with varying d_2 when $d_3 = 1.60\,\mu$m, $t_{ITO} = 15$ nm, and $t_{GOLD} = 30$ nm.

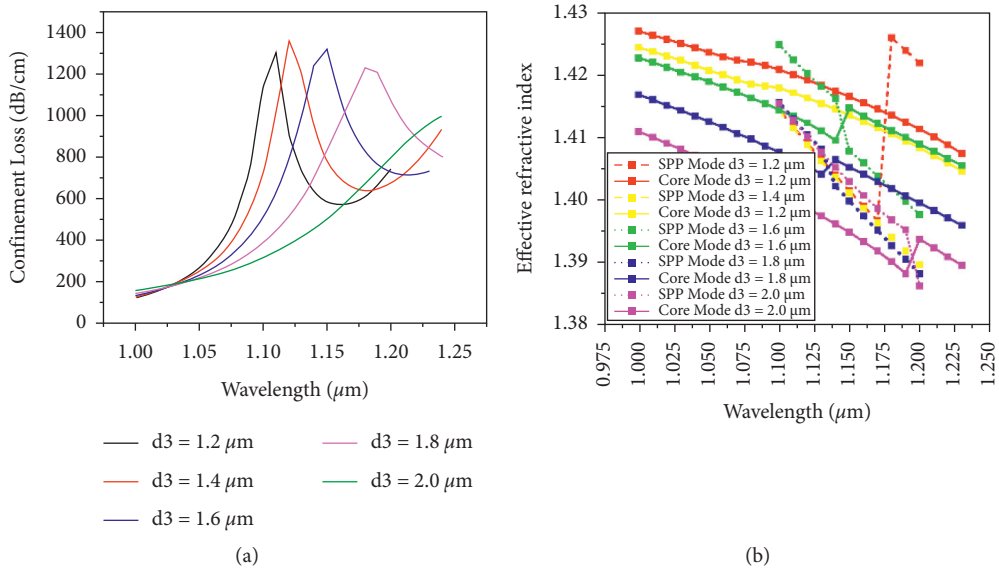

FIGURE 4: (a) Mode loss spectra and (b) the effective mode indices for various values of d_3 when $d_2 = 3.0\,\mu$m, $t_{ITO} = 15$ nm, and $t_{GOLD} = 30$ nm.

5 nm steps. The loss spectrum undergoes a blueshifts as t_{GOLD} increases.

When the phase-matching wavelengths are 1.23 μm, 1.20 μm, 1.15 μm, 1.11 μm, and 1.09 μm, the corresponding losses are 1650.00 dB/cm, 1578.603 dB/cm, 1319.609 dB/cm, 1148.549 dB/cm, and 1065.929 dB/cm, respectively. At lower t_{GOLD} values, the corresponding losses are lower allowing effective interaction with the core-guided modes. However, higher t_{GOLD} values produced higher losses due to plasmonic damping losses [33].

3.3. Impact of ITO Thickness on the Filter's Response. The influence of t_{ITO} is investigated at this point. The corresponding loss spectra depicting the response of the

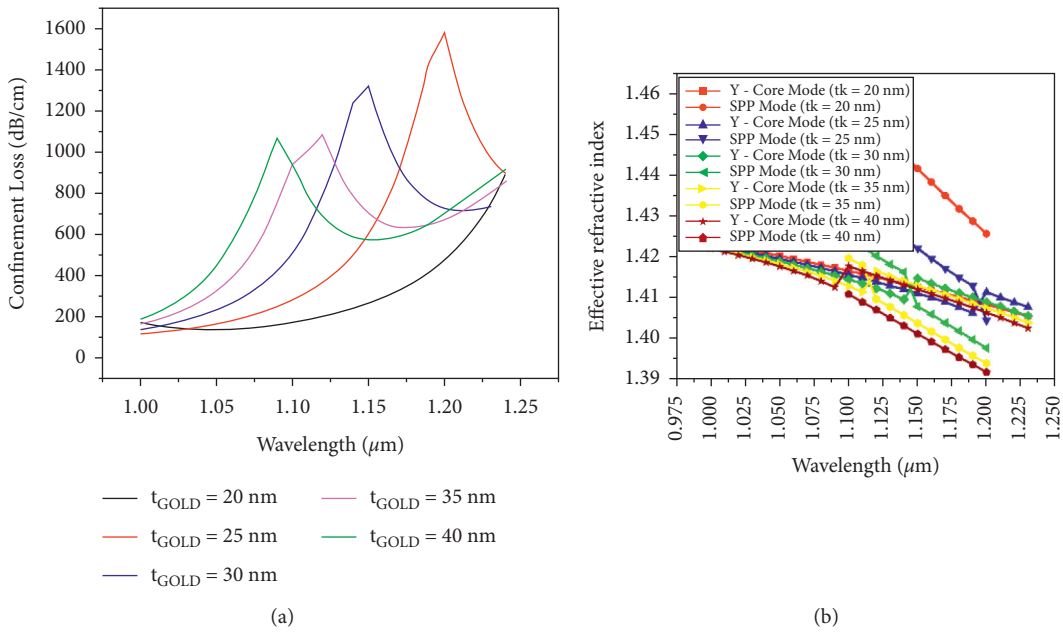

Figure 5: Differences in the loss spectra for the filter model with varied t_{GOLD}.

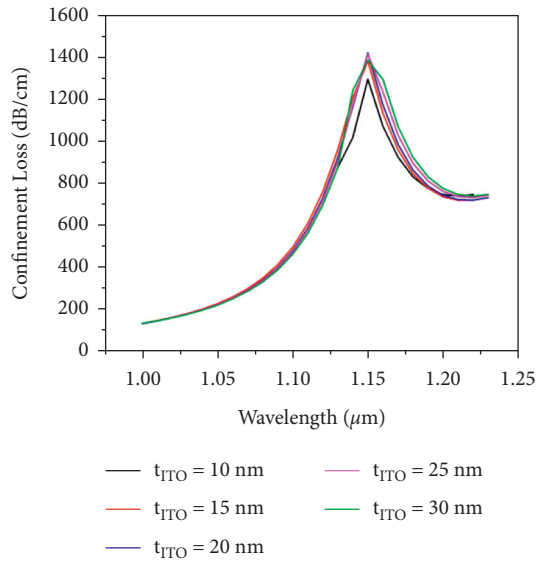

Figure 6: Differences in the loss spectra for the filter model with varied t_{ITO}.

proposed filter are shown in Figure 6 in 5 nm steps. The peak shift is not affected by the loss t_{ITO} thicknesses. The overall confinement loss increases for ITO thickness up to 30 nm and thereafter tends to decrease. The lowest losses of the ITO coating correspond the lowest thickness at $t_{ITO} = 10$ nm. Conversely, higher t_{ITO} thicknesses produces higher losses. Since higher t_{ITO} values introduces higher damping losses [33], the filter performs better at higher t_{ITO}.

As the confinement losses are significantly unchanged from $t_{ITO} = 10$ nm to $t_{ITO} = 30$ nm, we have confined our analysis to $t_{ITO} = 15$ nm for further analysis. The reason was to avert the influence of t_{ITO} on t_{GOLD}.

3.4. Crosstalk Analysis of the Proposed Filter. Crosstalk (CT) is another key characteristic that defines the effect of undesired polarized modes that can be used to assess the filter's transmission performance. As a function of fiber length, the CT can be stated as follows [13]:

$$CT = 20\lg\{\exp[(\alpha_2 - \alpha_1) \times L]\}, \quad (5)$$

where α_1, α_2, and L denote the length of the filter and the loss of the x- and y-polarized core modes, respectively. Figure 7 describes the CT variants for the filter model with various values of L when $t_{GOLD} = 30$ nm, $t_{GOLD} = 40$ nm, and $t_{GOLD} = 50$ nm, respectively. The length, L, of the filter was increased from 0.25 mm to 1 mm for the specified gold film

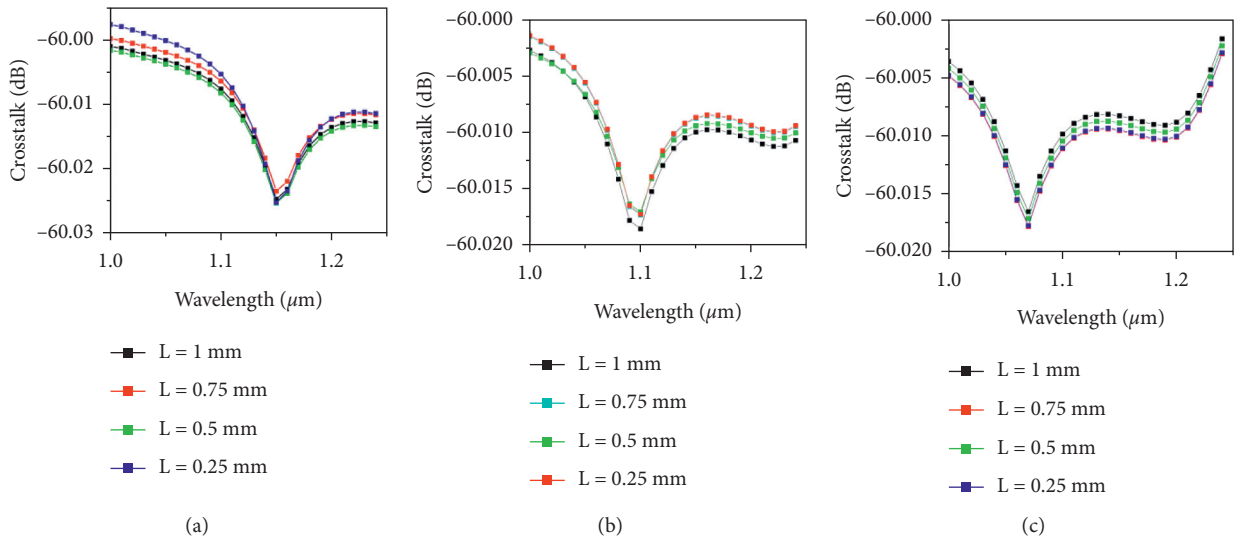

Figure 7: Crosstalk variations under changing fiber length L when (a) $t_{GOLD} = 30$ nm, (b) $t_{GOLD} = 40$ nm, and (c) $t_{GOLD} = 50$ nm.

thicknesses. The dependence of CT on the wavelength for the filter lengths is shown in Figures 7(a)–7(c).

In Figure 7(a), the magnitudes of the CT values are 60.0012, 62.499, 66.0217, and 72.0423752, respectively. The bandwidth reaches up to 602 nm. In Figure 7(b), they are 60.018, 62.517, 66.039, and 72.059, respectively, and the bandwidth is up to 600 nm. Finally, in Figure 7(c), the values of the CT are 60.016, 62.516, 66.037, and 72.0577, respectively, with a bandwidth of 601 nm. The obtained optical bandwidths are at the wavelength range beyond −20 dB. The CT can reach to 72.05 dB at a wavelength of 1150 nm at multiple fiber lengths of 30 mm, 40 mm, and 50 mm.

4. Conclusion

A single-polarization PCF filter based on PCF with layers of plasmonic gold and ITO has been proposed in this study. The filter can easily be fabricated using current precision ultrasonic drilling technique. The FEM solver in COMSOL® Multiphysics was used to analyze its characteristics. The proposed PCF filter is well suited for single-polarization filtering since the loss of the x-polarized core mode is significantly lower than that of the y-polarized mode at a communication wavelength. At a communication window of 1.55 μm, an excellent filtering effect was obtained by selecting optimal structural parameters and plasmonic film thicknesses of gold and ITO. When the filter is 1 mm long, the obtained filtering effect is 1319.689 dB/cm for the y-polarization and 31.881 dB/cm for the x-polarization, thus efficiently attenuating the y-component at a communication window of 1.15 μm. With a filtering bandwidth of 602 nm, the proposed filter shows superior characteristics compared with previously reported results. The plasmonic PCF filter would be extensively useful in polarization state management and polarization suppression systems for optical sensing and broadband transmission.

Data Availability

The data set is available from the author upon request through email.

Conflicts of Interest

The authors declare that they have no conflicts of interest.

References

[1] B. K. Paul, F. Ahmed, M. G. Moctader, K. Ahmed, and D. Vigneswaran, "Silicon nano crystal filled photonic crystal fiber for high nonlinearity," *Optical Materials*, vol. 84, pp. 545–549, 2018.

[2] B. K. Paul, K. Ahmed, M. Thillai Rani, K. P. Sai Pradeep, and F. A. Al-Zahrani, "Ultra-high negative dispersion compensating modified square shape photonic crystal fiber for optical broadband communication," *Alexandria Engineering Journal*, vol. 61, no. 4, pp. 2799–2806, 2022.

[3] X. Lu, M. Chang, N. Chen, X. Zhang, S. Zhuang, and J. Xu, "Design of a metal-filled photonic-crystal fiber polarization filter based on surface plasmon resonance at 1.31 and 1.55 μ m," *IEEE Photonics Journal*, vol. 10, no. 5, pp. 1–13, 2018.

[4] M. Chang, B. Li, N. Chen, X. Lu, X. Zhang, and J. Xu, "A compact and broadband photonic crystal fiber polarization filter based on a plasmonic resonant thin gold film," *IEEE Photonics Journal*, vol. 11, no. 2, pp. 1–12, 2019.

[5] B. K. Paul, K. Ahmed, S. Asaduzzaman, and M. S. Islam, "Folded cladding porous shaped photonic crystal fiber with high sensitivity in optical sensing applications: design and analysis," *Sensing and Bio-Sensing Research*, vol. 12, pp. 36–42, 2017.

[6] B. K. Paul, E. Rajesh, S. Asaduzzaman et al., "Design and analysis of slotted core photonic crystal fiber for gas sensing application," *Results in Physics*, vol. 11, pp. 643–650, 2018.

[7] M. N. Hossen, M. Ferdous, K. Ahmed, M. A. Khalek, S. Chakma, and B. K. Paul, "Single polarization photonic crystal fiber filter based on surface plasmon resonance," *Frontiers of Optoelectronics*, vol. 12, no. 2, pp. 157–164, 2019.

[8] Y.-W. Ma, Z.-W. Wu, L.-H. Zhang, J. Zhang, G.-S. Jian, and S. Pan, "Theoretical study of the local surface plasmon resonance properties of silver nanosphere clusters," *Plasmonics*, vol. 8, no. 3, pp. 1351–1360, 2013.

[9] G. An, S. Li, W. Qin, W. Zhang, Z. Fan, and Y. Bao, "High-sensitivity refractive index sensor based on D-shaped photonic crystal fiber with rectangular lattice and nanoscale gold film," *Plasmonics*, vol. 9, no. 6, pp. 1355–1360, 2014.

[10] W. Zhang, Z. Zhang, Y. Liu et al., "Design for a single-polarization photonic crystal fiber wavelength splitter based on hybrid-surface plasmon resonance," *IEEE Photonics Journal*, vol. 6, no. 4, pp. 1–9, 2014.

[11] X. Zhang, R. Wang, F. M. Cox, B. T. Kuhlmey, and M. C. J. Large, "Selective coating of holes in microstructured optical fiber and its application to in-fiber absorptive polarizers," *Optics Express*, vol. 15, no. 24, Article ID 16270, 2007.

[12] J. Lou, T. Cheng, and S. Li, "Plasma dual-wavelength single polarizing filter with gold film and liquid-filled air hole based on photonic crystal fiber," *Optik*, vol. 165, pp. 295–301, 2018.

[13] Y. Zhao, S. Li, Q. Liu, and X. Wang, "Design of a novel photonic crystal fiber filter based on gold-coated and elliptical air holes," *Optical Materials*, vol. 73, pp. 638–641, 2017.

[14] X. Feng, S. Li, H. Du, Y. Zhang, and Q. Liu, "A simple gold-coated microstructure fiber polarization filter in two communication windows," *Optical Fiber Technology*, vol. 41, pp. 74–77, 2018.

[15] H. Reddy, U. Guler, Z. Kudyshev, A. v. Kildishev, V. M. Shalaev, and A. Boltasseva, "Temperature-dependent optical properties of plasmonic titanium nitride thin films," *ACS Photonics*, vol. 4, no. 6, pp. 1413–1420, 2017.

[16] J. Lou, S. Li, T. Cheng, X. Yan, X. Zhang, and Y. Shao, "Polarization filter based on plasmonic photonic crystal fiber with asymmetry around Au-coated and liquid-filled air holes," *Optik*, vol. 149, pp. 162–168, 2017.

[17] X. Feng, T. Astell-Burt, W. C. Sullivan, and C.-Y. Chang, "The relationship between neighbourhood green space and child mental wellbeing depends upon whom you ask: multilevel evidence from 3083 children aged 12-13 years," *International Journal of Environmental Research and Public Health*, vol. 14, no. 3, p. 235, 2017.

[18] Y. Du, S.-G. Li, S. Liu, X.-P. Zhu, and X.-X. Zhang, "Polarization splitting filter characteristics of Au-filled high-birefringence photonic crystal fiber," *Applied Physics B*, vol. 109, no. 1, pp. 65–74, 2012.

[19] G. An, S. Li, X. Yan, Z. Yuan, and X. Zhang, "High-birefringence photonic crystal fiber polarization filter based on surface plasmon resonance," *Applied Optics*, vol. 55, no. 6, p. 1262, 2016.

[20] Z. Fan, S. Li, H. Chen et al., "Numerical analysis of polarization filter characteristics of D-shaped photonic crystal fiber based on surface plasmon resonance," *Plasmonics*, vol. 10, no. 3, pp. 675–680, 2015.

[21] M. Li, L. Peng, G. Zhou, B. Li, Z. Hou, and C. Xia, "Design of photonic crystal fiber filter with narrow width and single-polarization based on surface plasmon resonance," *IEEE Photonics Journal*, vol. 9, no. 3, pp. 1–8, 2017.

[22] Y. Liu, X. Jing, S. Li et al., "Design of a single-polarization filter based on photonic crystal fiber with gold film on the inner wall of two ultra-large holes," *Optics and Laser Technology*, vol. 114, pp. 114–121, 2019.

[23] B. H. Almewafy, N. F. F. Areed, and M. F. O. Hameed, "Multifunctional surface plasmon resonance photonic-crystal fiber polarization filter at telecommunication wavelengths," *Journal of Nanophotonics*, vol. 13, no. 01, p. 1, 2019.

[24] R. T. Bise, D. J. Trevor, R. T. Bise, and D. J. Trevor, "Sol-gel derived microstructured fiber: fabrication and characterization," in *Proceedings of the OFC/NFOEC Technical Digest. Optical Fiber Communication Conference, 2005*, IEEE, Anaheim, CA, USA, Mar 2005.

[25] C. Yi, P. Zhang, F. Chen et al., "Fabrication and characterization of Ge20Sb15S65 chalcogenide glass for photonic crystal fibers," *Applied Physics B*, vol. 116, no. 3, pp. 653–658, 2014.

[26] S. An, J. Lv, Z. Yi et al., "Ultra-short and dual-core photonic crystal fiber polarization splitter composed of metal and gallium arsenide," *Optik*, vol. 226, Article ID 165779, 2021.

[27] J.-P. Berenger, "A perfectly matched layer for the absorption of electromagnetic waves," *Journal of Computational Physics*, vol. 114, 1994.

[28] X. Feng, H. Du, S. Li, Y. Zhang, Q. Liu, and X. Gao, "A broadband core shift polarization filter based on photonic crystal fiber with a big gold-coated air hole," *Optical and Quantum Electronics*, vol. 49, no. 7, pp. 1–9, 2017.

[29] G. An, S. Li, W. Zhang, Z. Fan, and Y. Bao, "A polarization filter of gold-filled photonic crystal fiber with regular triangular and rectangular lattices," *Optics Communications*, vol. 331, pp. 316–319, 2014.

[30] A. Forouzmand, M. M. Salary, G. Kafaie Shirmanesh, R. Sokhoyan, H. A. Atwater, and H. Mosallaei, "Tunable all-dielectric metasurface for phase modulation of the reflected and transmitted light via permittivity tuning of indium tin oxide," *Nanophotonics*, vol. 8, no. 3, pp. 415–427, 2019.

[31] T. P. White, R. C. Mcphedran, C. M. De Sterke, L. C. Botten, and M. J. Steel, "Confinement losses in microstructured optical fibers," *Optics Letter*, vol. 26, 2001.

[32] Q. Liu, S. Li, H. Li et al., "Broadband single-polarization photonic crystal fiber based on surface plasmon resonance for polarization filter," *Plasmonics*, vol. 10, no. 4, pp. 931–939, 2015.

[33] N. Liu, L. Langguth, T. Weiss et al., "Plasmonic analogue of electromagnetically induced transparency at the Drude damping limit," *Nature Materials*, vol. 8, no. 9, pp. 758–762, 2009.